SIAM J. SCI. COMPUT.
Vol. 23, No. 5, pp. 1485–1502

MULTIDIMENSIONAL LEAST SQUARES FLUCTUATION DISTRIBUTION SCHEMES WITH ADAPTIVE MESH MOVEMENT FOR STEADY HYPERBOLIC EQUATIONS*

M. J. BAINES†, S. J. LEARY‡, AND M. E. HUBBARD§

Abstract. Optimal meshes and solutions for steady conservation laws and systems within a finite volume fluctuation distribution framework are obtained by least squares methods incorporating mesh movement. The problem of spurious modes is alleviated through adaptive mesh movement, the least squares minimization giving an obvious way of determining the movement of the nodes and also providing a link with equidistribution. The iterations are carried out locally node by node, which yields good control of the moving mesh. For scalar equations an iteration which respects the flow of information in the problem significantly accelerates the convergence.

The method is demonstrated on a scalar advection problem and a shallow water channel flow problem. For discontinuous solutions we introduce a least squares shock fitting approach which greatly improves the treatment of discontinuities at little extra expense by using degenerate triangles and moving the nodes. Examples are shown for a discontinuous shallow water channel flow and a shocked flow in gasdynamics governed by the compressible Euler equations.

Key words. least squares, fluctuation distribution, mesh movement, hyperbolic equations

AMS subject classification. 76M12

PII. S1064827500370202

1. Introduction.

Finite volume schemes of fluctuation distribution type for the approximation of steady first order hyperbolic equations and systems are now well established. In particular, the class of multidimensional upwind schemes on unstructured triangular meshes has been very successful [13]. The least squares methods of finite volume type discussed in this paper also belong to this family, although their properties differ.

Roe was the first to suggest the fluctuation-distribution framework for steady first order hyperbolic PDEs and systems in multidimensions [10]. In this approach a fluctuation (proportional to the PDE residual) is defined on each cell of the mesh and distributed by signals to the nodes of the cell; i.e., weighted fractions of the fluctuation are added to the solution values at the nodes of the cell. This distribution is carried out for each cell, and the cumulative update at a node is the sum of the weighted contributions from cells with that node as a target. To reach steady state the procedure is repeated, updating the solution values until the total increments at every node have become zero, at which point the process is said to have converged.

As pointed out in [11], a descent method applied to the least squares method within a finite volume framework is also a fluctuation-distribution scheme. In the

*Received by the editors April 5, 2000; accepted for publication (in revised form) February 21, 2001; published electronically January 4, 2002.
http://www.siam.org/journals/sisc/23-5/37020.html

†Department of Mathematics, P.O. Box 220, Reading, RG6 6AX, UK (M.J.Baines@reading.ac.uk). The work of the first author was supported by a research grant from the Engineering and Physical Science Research Council (EPSRC).

‡Department of Engineering, University of Southampton, Southampton, S017 IBJ, UK (S.J.Leary@soton.ac.uk). The work of the second author was supported by a Collaborative Awards in Science and Engineering (CASE) studentship.

§Department of Computer Science, University of Leeds, Leeds, LS2 9JT, UK (meh@comp.leeds.ac.uk). The work of the third author was supported by a research grant from the Engineering and Physical Science Research Council (EPSRC).

present paper this idea is developed further, using among other things the connection between least squares minimization and equidistribution [1], and in particular is extended to nonlinear systems of PDEs.

For fluctuation distribution schemes in general, even though the total increments at a node may have converged to zero, the individual cell residuals (or fluctuations) need not have vanished but only their weighted sums, leading sometimes to an unsatisfactory solution. One way to alleviate the difficulty is to increase the number of degrees of freedom available by including the mesh locations as additional variables in the least squares minimization and hence moving the mesh. As a consequence, when the total increments at a node converge, the individual fluctuations in a cell are closer to zero and yield a better approximation to the PDE and the solution. In the case of scalar problems, spurious solutions may be eliminated altogether and the outcome identified with an approximate method of characteristics.

Repositioning the nodes in this way leads to conservation and a measure of equidistribution, the latter ensuring that convergence takes place uniformly with respect to the mesh.

In this paper the method is applied to a scalar PDE problem and a shallow water channel flow problem, both of whose solutions are smooth.

For problems with nonsmooth solutions, least squares methods are known to give poor solutions close to discontinuities. Here we take a shock fitting approach and use a least squares moving mesh method to improve the position of the shock. In recent years a great deal of effort has been put into mesh refinement near shocks using mesh subdivision, but substantial improvements in shock resolution can also be obtained by making minor adjustments to the mesh. We introduce degenerate cells in the vicinity of the shock and a least squares shock fitting procedure to adjust its position. A multidimensional upwinding shock capturing scheme [13] is used to generate an initial solution and a first approximation to the position of the shock. A least squares shock fitting approach is then used to improve the position of the shock [4], [7]. This is achieved by a least squares minimization of a measure of the jump condition over nodal positions in degenerate cells. In the smooth regions on either side of the shock the least squares method may then be expected to work well.

Results are shown for a scalar problem with a contact discontinuity, a shallow water problem in a constricted channel with a hydraulic jump, and an Euler gasdynamics problem with an exact solution, including a shock reflection.

The layout of the paper is as follows. In section 2 we give the definition of the fluctuation and its functional form in certain cases. Section 3 describes fluctuation distribution schemes and least squares methods (with descent) in a finite volume framework. In section 4 we discuss the role of node movement in improving the accuracy of solutions and exploiting the link between least squares and equidistribution. Details of the descent methods used for achieving least squares minima are described in section 5, and an upwinding strategy is described in section 6. Results are shown in section 7 for a scalar advection example and a problem involving a nonlinear system of equations, the Shallow Water Equations.

The role of degenerate cells in generating discontinuous solutions is discussed in section 8. Results for some discontinuous scalar problems and nonlinear systems are shown in section 9 with conclusions in section 10.

2. Fluctuations. We consider the two-dimensional conservation law

$$\operatorname{div}(\underline{f}(u)) = 0 \tag{2.1}$$

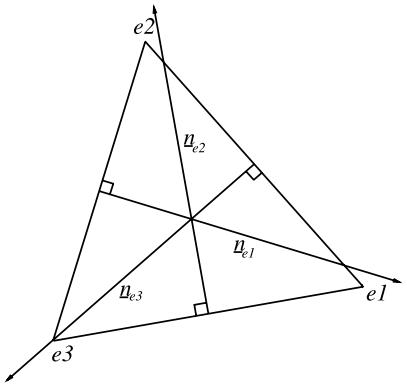

FIG. 1. *A general triangular cell e.*

with integral form

$$\oint_\Gamma \underline{f}(u).\underline{\hat{n}}d\Gamma = 0, \tag{2.2}$$

where $\underline{\hat{n}}$ is the inward normal to an arbitrary closed surface Γ in a domain Ω. The boundary condition is an inflow condition over Γ_1, the part of the surface for which $\frac{\partial f}{\partial u}.\underline{\hat{n}} \geq 0$.

Let the domain be divided into triangles Ω_e, and let $\underline{f}$ be approximated by a piecewise linear function $\underline{F}$. Then we define the fluctuation in triangle Ω_e to be

$$\phi_e = \oint_{\Gamma_e} \underline{F}.\underline{\hat{n}}d\Gamma, \tag{2.3}$$

where Γ_e is the perimeter of Ω_e.

We also define the average residual

$$\overline{R}_e = \frac{1}{S_e}\int_{\Omega_e} \mathrm{div}\underline{F}d\Omega = \frac{1}{S_e}\oint_{\Gamma_e} \underline{F}.\underline{\hat{n}}d\Gamma = \frac{\phi_e}{S_e}, \tag{2.4}$$

where S_e is the area of triangle e.

Since $\underline{F}$ is linear in the triangle we can use a trapezium rule quadrature to write (2.3) as

$$\phi_e = \frac{1}{2}\left\{(\underline{F}_{e1}+\underline{F}_{e2}).\underline{n}_{e3} + (\underline{F}_{e2}+\underline{F}_{e3}).\underline{n}_{e1} + (\underline{F}_{e3}+\underline{F}_{e1}).\underline{n}_{e2})\right\}, \tag{2.5}$$

where $\underline{n}_{ei}$ $(i = 1, 2, 3)$ is the inward unit normal to the ith edge of triangle e (opposite the vertex ei), as shown in Figure 1, multiplied by the length of that edge. It is easy to verify that, for any triangle,

$$\underline{n}_{e1} + \underline{n}_{e2} + \underline{n}_{e3} = 0, \tag{2.6}$$

so the fluctuation (2.5) may be written as

$$\phi_e = -\frac{1}{2}\left\{\underline{F}_{e1}.\underline{n}_{e1} + \underline{F}_{e2}.\underline{n}_{e2} + \underline{F}_{e3}.\underline{n}_{e3}\right\}, \tag{2.7}$$

or, since $\underline{n}_{ei} = (\Delta Y_{ei}, -\Delta X_{ei})$,

$$\phi_e = -\frac{1}{2}\sum_{ei=1}^{3}\left(F_{ei}\Delta Y_{ei} - G_{ei}\Delta X_{ei}\right), \tag{2.8}$$

where $\underline{F} = (F, G)$ and $\Delta_{e1}X = X_{e2} - X_{e3}$ denotes the difference in X taken across the side opposite node $e1$ in a counterclockwise sense (and similarly for $\Delta_{e2}X$ and $\Delta_{e3}X$). A dual form of the fluctuation is obtained by rewriting (2.7) as

$$\phi_e = \frac{1}{2}\sum_{ei=1}^{3}\left(Y_{ei}\Delta F_{ei} - X_{ei}\Delta G_{ei}\right). \tag{2.9}$$

We aim to set the fluctuations ϕ_e to zero in order to satisfy (2.1).

In the case where $\underline{f}$ is of the form

$$\underline{f} = \underline{a}(\underline{x})u, \tag{2.10}$$

where $\underline{a}(\underline{x})$ is a divergence-free velocity field, the PDE (2.1) reduces to the advection equation

$$\underline{a}(\underline{x}).\underline{\nabla}u = 0. \tag{2.11}$$

Then the fluctuation may be written

$$\phi_e = -\frac{1}{2}\sum_{ei=1}^{3}\left(a_{ei}U_{ei}\Delta Y_{ei} - b_{ei}U_{ei}\Delta X_{ei}\right), \tag{2.12}$$

where $\underline{a} = (a, b) = (a(X_{ei}, Y_{ei}), b(X_{ei}, Y_{ei}))$.

Now consider systems of nonlinear hyperbolic equations

$$\mathrm{div}\underline{\mathbf{f}}(\mathbf{u}) = 0 = \underline{A}(\mathbf{u}).\underline{\nabla}\mathbf{u}, \tag{2.13}$$

where $\underline{A}$ is a vector of the Jacobian matrices $(A, B)^T$. The integral form is

$$\oint_{\Gamma}\underline{\mathbf{f}}(\mathbf{u}).\underline{\hat{n}}d\Gamma = 0, \tag{2.14}$$

and the fluctuation (with $\mathbf{f}$ approximated by $\mathbf{F}$) is

$$\boldsymbol{\phi}_e = -\frac{1}{2}\left(\underline{\mathbf{F}}_{e1}.\underline{n}_{e1} + \underline{\mathbf{F}}_{e2}.\underline{n}_{e2} + \underline{\mathbf{F}}_{e3}.\underline{n}_{e3}\right) \tag{2.15}$$

$$= -\frac{1}{2}\sum_{ei=1}^{3}\left(\mathbf{F}_{ei}\Delta Y_{ei} - \mathbf{G}_{ei}\Delta X_{ei}\right) \tag{2.16}$$

with dual form

$$\boldsymbol{\phi}_e = \frac{1}{2}\sum_{ei=1}^{3}\left(Y_{ei}\Delta\mathbf{F}_{ei} - X_{ei}\Delta\mathbf{G}_{ei}\right). \tag{2.17}$$

Two systems of interest are the Euler equations of gasdynamics and the Shallow Water Equations.

3. Fluctuation distribution schemes and least squares. In fluctuation distribution schemes we seek to set the fluctuations ϕ_e to zero via an iterative procedure with an index n, say. In this procedure the ϕ_e^n, obtained by substituting an estimate U^n into the (F, G) in (2.8), are distributed to nodes of the mesh in order to give a U^{n+1} for which the ϕ_e^{n+1} are smaller. At each stage of the iteration, for each triangle Ω_e, a weighted amount of ϕ_e is added to the values of the solution at the vertices of the triangle. In the multidimensional upwind schemes [13], [8] the weights are chosen so that the schemes are conservative, positive, and linearity preserving. Conservation is ensured if the weights in each triangle sum to unity.

In the least squares descent method we seek to minimize either the L_2 norm of the average residual (see (2.4)) or the l_2 norm of the vector of fluctuations, using a gradient descent method. This l_2 norm is useful since it is bounded even for the degenerate triangles considered in section 7.

The square of the L_2 norm of the average residual, from (2.4), is

$$\mathcal{F}_1 = \sum_e \int_{\Omega_e} \overline{R}_e^2 d\Omega = \sum_e S_e \overline{R}_e^2 = \sum_e \frac{\phi_e^2}{S_e}, \tag{3.1}$$

or, in the systems case,

$$\mathcal{F}_1 = \sum_e \frac{\boldsymbol{\phi}_e^t \boldsymbol{\phi}_e}{S_e} \tag{3.2}$$

(cf. [11]). For the l_2 norm of the vector of fluctuations we have

$$\mathcal{F}_2 = \sum_e \phi_e^2 \qquad \text{or} \qquad \mathcal{F}_2 = \sum_e \boldsymbol{\phi}_e^t \boldsymbol{\phi}_e \tag{3.3}$$

in the systems case.

Using a gradient descent method to carry out the minimization, we find that each step adds weighted amounts of the ϕ_e in each triangle to the values of the solution at the vertices of the triangle and hence has the form of a fluctuation distribution scheme. For example, in the $\mathcal{F}_2$ case, since the gradient of ϕ_e^2 with respect to the nodal value U_j is

$$\left\{ 2 \frac{\partial \phi_e}{\partial U_j} \right\} \phi_e \tag{3.4}$$

a descent method will add a multiple of ϕ_e to U_j. The weight (in the curly bracket), from (2.8), is

$$w_{je} = 2 \frac{\partial \phi_e}{\partial U_j} = -\frac{\partial}{\partial U_j} \sum_{ei=1}^{3} \{ F_{ei} \Delta Y_{ei} - G_{ei} \Delta X_{ei} \} \tag{3.5}$$

$$= -\frac{dF_{je}}{dU_{je}} \Delta Y_{je} + \frac{dG_{je}}{dU_{je}} \Delta X_{je} \tag{3.6}$$

$$= -a(U_{je}) \Delta Y_{je} + b(U_{je}) \Delta X_{je}, \tag{3.7}$$

where je is the node of triangle e corresponding to j and we have used

$$(a(U), b(U)) = \left(\frac{dF}{dU}, \frac{dG}{dU} \right). \tag{3.8}$$

In the case of differentiation with respect to $\underline{X}_j$, the gradient of ϕ_e^2 is

$$\left\{2\frac{\partial \phi_e}{\partial \underline{X}_j}\right\}\phi_e \tag{3.9}$$

and a descent method will add a multiple of ϕ_e to $\underline{X}_j$. This time the vector weights, using (2.17), are

$$\underline{w}_{je} = (0,1)^T \Delta F_{je} + (-1,0)^T \Delta G_{je}. \tag{3.10}$$

For systems of equations the corresponding matrix weights corresponding to (3.7) and (3.10) are

$$W_{je} = -A(\mathbf{U}_{je})\Delta Y_{je} + B(\mathbf{U}_{je})\Delta X_{je} \tag{3.11}$$

and

$$\underline{W}_{je} = (0,1)^T \Delta \mathbf{F}_{je} + (-1,0)^T \Delta \mathbf{G}_{je}. \tag{3.12}$$

For the advection equation (2.10) we have from (2.12) the weights

$$w_{je} = -a(X_{je}, Y_{je})\Delta Y_{je} + b(X_{je}, Y_{je})\Delta X_{je} \tag{3.13}$$

for U variations and, using a dual form of (2.12),

$$\underline{w}_{je} = \frac{\partial}{\partial \underline{X}_j} \sum_{ei=1}^{3} - \left\{\Delta\left(a(X_{ei}, Y_{ei})U_{ei}\right) Y_{ei} + \Delta\left(b(X_{ei}, Y_{ei})U_{ei}\right) X_{ei}\right\} \tag{3.14}$$

for the $\underline{X}$ variations.

Similar sets of weights may be found in the minimization of $\mathcal{F}_1$. In particular, (3.9) generalizes to

$$\frac{\partial}{\partial \underline{X}_j}\left(\frac{\phi_e^2}{S_e}\right) = \left\{\frac{2}{S_e}\frac{\partial \phi_e}{\partial \underline{X}_j} - \frac{\phi_e}{S_e^2}\frac{\partial S_e}{\partial \underline{X}_j}\right\}\phi_e. \tag{3.15}$$

4. Moving the nodes. There are two motivations for moving the nodes. The first is the problem of spurious solutions. The number of equations given by (2.3) is equal to the number of triangles in the mesh, but the number of unknowns is a multiple of the number of nodes. In general these are different. If the number of equations exceeds the number of unknowns it is impossible to satisfy all the equations. For any iteration of fluctuation distribution type in which fluctuations are added to the vertices of the mesh with weights, convergence of the nodal updates does not imply that the fluctuations vanish. In particular, in the least squares descent approach the norms (3.1), (3.3) are not necessarily driven down to zero. However, if we allow the coordinates of the vertices to become additional unknowns of the problem, the number of degrees of freedom is increased and the solution is improved.

For scalar problems the number of unknowns then exceeds the number of equations and there are infinitely many solutions which make the norms zero. A unique solution is obtained if the number of unknowns is equal to the number of equations, and this may be achieved in a scalar problem by including just one coordinate per node in the list of unknowns. The fluctuations may then be driven to zero by a

fluctuation-distribution scheme. The result is an approximate method of characteristics, as in Example 1 below. The accuracy of the approximate solution depends only on the coarseness and/or connectivity of the mesh. For a system of two equations in two dimensions, the number of unknowns is equal to the number of equations when the nodes are allowed to move in both directions, and this has been studied in [11]. For systems such as the Shallow Water or the Euler Equations of gasdynamics the number of equations is always less than or equal to the number of unknowns, but the inclusion of nodal variables significantly increases the number of degrees of freedom.

The second motivation comes from a link with equidistribution. As in [1], the identity

$$\left(\sum_e S_e\right)\left(\sum_e S_e \bar{R}_e^2\right) = \left(\sum_e \phi_e\right)^2 + \sum_{e_1>e_2} S_{e_1} S_{e_2} \left(\bar{R}_{e_1} - \bar{R}_{e_2}\right)^2 \tag{4.1}$$

shows that, if the total area of the domain $\sum_e S_e$ is fixed, then driving the norm $\mathcal{F}_1$ (which from (3.1) equals $\sum_e S_e \bar{R}_e^2$) down to zero forces both terms on the right-hand side of (4.1) to zero, resulting in both global conservation and residual "equidistribution." The first follows because of the cancellation property

$$\phi = \sum_e \phi_e = \frac{1}{2} \sum_e \sum_{ei=1}^{3} \left(-F_{ei}\Delta Y_{ei} + G_{ei}\Delta X_{ei}\right) \tag{4.2}$$

$$= \frac{1}{2} \sum_b \left(-F_b \Delta Y_b + G_b \Delta X_b\right), \tag{4.3}$$

so that the total ϕ over the domain is equal to a sum over boundary values b only. Hence the first term on the right-hand side of (4.1) is a measure of global conservation, while the second term is a measure of equidistribution of the average residual $\overline{R}_e$.

In a similar way the identity

$$\left(\sum_e 1\right)\left(\sum_e \phi_e^2\right) = \left(\sum_e \phi_e\right)^2 + \sum_{e_1>e_2} \left(\phi_{e_1} - \phi_{e_2}\right)^2 \tag{4.4}$$

(see [1]) ensures that, provided that the number of triangles $\sum_e 1$ remains fixed, the act of driving the norm $\sum_e \phi_e^2$ down to zero also forces global conservation and a measure of equidistribution of the fluctuations ϕ_e to go to zero. These statements generalize immediately to systems of equations.

The global conservation term (4.3) is evidently unaffected by any adjustment to the values at the interior nodes. Therefore a reduction in the sum of squares term on the left-hand side of (4.1) or (4.4) due to such adjustments simply serves to improve the quality of the equidistribution.

We shall discuss the use of least squares descent methods as fluctuation distribution schemes in this context. Unlike multidimensional upwinding [2], such an approach has the advantage of a norm to minimize which can readily be used to generate the movement of the mesh as well as inducing global conservation and equidistribution in the sense described above.

5. The descent methods. We give now the details of the minimization of $\mathcal{F}_2$ with respect to the nodal values U_j and coordinates $\underline{X}_j$, using a gradient descent

method. The steepest descent method generates contributions from the set of triangles je surrounding node j, to be added to the values of U_j and $\underline{X}_j$, of the form

$$\delta U_j = -\tau_2 \sum_{je} \left\{ 2 \frac{\partial \phi_{je}}{\partial U_j} \right\} \phi_{je}, \qquad \delta \underline{X}_j = -\sigma_2 \sum_{je} \left\{ 2 \frac{\partial \phi_{je}}{\partial \underline{X}_j} \right\} \phi_{je} \tag{5.1}$$

(see (3.4) and (3.9)), where τ_2 and σ_2 are suitably chosen relaxation factors, and the negative sign ensures that we go down the gradient. The relaxation parameters control the step taken in the descent direction and are generally chosen via a line search or a local quadratic model. Sometimes, however, it is necessary to take an empirical approach to the choices of these factors.

In this paper we use a splitting technique, first minimizing $\mathcal{F}_2$ with respect to U_j with $\underline{X}_j$ held constant and then minimizing $\mathcal{F}_2$ with respect to $\underline{X}_j$ with U_j held constant. (It is possible, though unlikely, that the constrained nature of the minimization may lead to a saddle point.)

Consequently, for the minimization over U we may construct a quadratic model in which the relaxation parameter is

$$\left(\frac{\partial^2 \mathcal{F}_2}{\partial U_j^2} \right)^{-1} = \left(\frac{\partial^2}{\partial U_j^2} \sum_{je} \phi_{je}^2 \right)^{-1} \tag{5.2}$$

$$= \left(\frac{\partial^2}{\partial U_j^2} \sum_{je} \sum_{ei} \frac{1}{4} \underline{n}_{ei}^T \, \underline{F}_{ei} \underline{F}_{ei}^T \, \underline{n}_{ei} \right)^{-1} \tag{5.3}$$

by (2.7). Let us now linearize $\underline{F}_{ei}$ as $\underline{a}_{ei} U_{ei}$ so that the relaxation factor becomes

$$\left(\frac{\partial^2}{\partial U_j^2} \sum_{je} \sum_{ei} \frac{1}{4} \underline{n}_{ei}^T \, \underline{a}_{ei} U_{ei}^2 \underline{a}_{ei}^T \, \underline{n}_{ei} \right)^{-1} \tag{5.4}$$

$$= \left(\sum_{je} \frac{1}{4} \underline{n}_{je}^T \, \underline{a}_{je} \, \underline{a}_{je}^T \, \underline{n}_{je} \right)^{-1}. \tag{5.5}$$

For the $\underline{X}$ minimization of $\mathcal{F}_2$ the functional is already quadratic, giving the relaxation factor

$$\left(\frac{\partial^2 \mathcal{F}_2}{\partial \underline{X}_j^2} \right)^{-1} = \left(\frac{\partial^2}{\partial \underline{X}_j^2} \sum_{je} \sum_{ei} \frac{1}{4} \underline{F}_{ei}^T \, \underline{n}_{ei} \, \underline{n}_{ei}^T \, \underline{F}_{ei} \right)^{-1} \tag{5.6}$$

which is

$$= \left(- \sum_{je} \left(\underline{F}_{je1}^T \underline{F}_{je1} + \underline{F}_{je2}^T \underline{F}_{je2} \right) \right)^{-1} \tag{5.7}$$

for each coordinate, where $je1, je2$ are the vertices of the triangle je other than j. Alternatively, a line search may be carried out on each $\underline{X}_j$.

For the advection equation (2.10) a quadratic model may be obtained by freezing the advection speed in calculating the second derivative in the quadratic model (see (2.12)).

For the minimization of $\mathcal{F}_1$, rather than $\mathcal{F}_2$, we obtain an approximate quadratic model simply by inserting the factor S_{je}^{-1} between the a_{je}'s or A_{je}'s.

These choices generalize to systems of equations where (5.5) becomes

$$\left(\sum_{je} \frac{1}{4} \underline{n}_{je}^T \, \underline{A}_{je} \, \underline{A}_{je}^T \underline{n}_{je} \right)^{-1}, \tag{5.8}$$

where $\underline{A} = (A, B)$, and where $\underline{\mathbf{F}}$ has been linearized as $\underline{A}\mathbf{U}$.

The iterations are carried out by continually sweeping through the nodes of the mesh in a local manner. The identities (4.1) or (4.4) also hold on each patch of triangles surrounding a node, showing that least squares minimization leads to local conservation over the boundary of the patch and equidistribution over the triangles of the patch.

The sweeps through the nodes of the mesh may be carried out either in a Jacobi or a Gauss–Seidel manner. The local approach is helpful in controlling the mesh quality.

6. Upwinding. Generally, the rate of convergence is slow or very slow. However, we can show that in the scalar case convergence can be accelerated significantly by an awareness of the origin of the problem. One consequence of minimizing the least squares norm of the residual or the fluctuation of the equation $\underline{a}.\nabla u = 0$ is that the original equation is embedded in the second order degenerate elliptic equation $-\underline{a}.\nabla(\underline{a}.\nabla u) = 0$ (see e.g. [9]). The correct solution is picked out from the larger set of solutions by the outflow condition, which is the original differential equation $\underline{a}.\nabla u = 0$ applied at the outflow boundary. Indeed we may write the second order equation as the system

$$\underline{a}.\nabla u = v \tag{6.1}$$

with U given on Γ_2 and

$$-\underline{a}.\nabla v = 0 \tag{6.2}$$

with V given on Γ_1. The first of these is the solution of the original PDE with a source term v, which is the solution of the second equation. For the second equation the analytic solution is $v = 0$, but numerically a nonzero v will be generated building up from the outflow (the characteristics run backwards in (6.2)), forcing a nonzero source term in (6.1).

As befits an elliptic solver, the least squares descent method updates are distributed to all the nodes in a triangle, but it may be argued that, because of the hyperbolic nature of the original equation, the updates should exhibit an upwind bias, as in the case of multidimensional upwinding, and the nonzero v solution should be suppressed.

One way of achieving the upwind bias (see [3], [7]) is to carry out the minimization of the functional within each cell over only *downwind* nodal values. Furthermore, we allow temporary discontinuities in U at each node by letting the solution have one value associated with cells upwind of the node but another with downwind cells. The updates resulting from this minimization still reduce the functional but at the expense of making U discontinuous. However, we may follow this minimization step

by a second projection step which resets the *upwind* values of U so as to restore the continuity of U. This is not a descent step and may increase the fluctuation. Nevertheless, we may iterate on the two steps, seeking convergence. If convergence is attained the discontinuities have tended to zero, and we have a continuous U which also minimizes the functional since its gradient is zero. Since the minimization is constrained, a higher value of the functional may result (the two projections cancelling each other out), but further improvement may be found at this point by switching to the full least squares iteration.

By a similar argument on the dual form (2.9) of the fluctuation, the $\underline{X}$ contributions should also be upwinded (although the boundary conditions differ from those on v).

Not surprisingly we find that convergence is much faster, not only for the U variations but also for the $\underline{X}$ variations. The algorithm has a strong upwind bias which reflects the nature of the original problem and its dependence on characteristics. In fact the two steps taken together are equivalent to simply suppressing the upwind updates in the least squares descent method. With an appropriate scaling the U step is simply the Low Diffusion Scheme A (LDA) scheme of multidimensional upwinding [13].

We now give results for two problems in which these techniques are used.

7. Numerical results for continuous solutions.

Example 1. We first consider the scalar two-dimensional advection equation, considered in [11],

$$\underline{a}(\underline{x}).\nabla u = 0, \tag{7.1}$$

where $\underline{a}(\underline{x}) = (y, -x)$ in a rectangle $-1 \le x \le 1, 0 \le y \le 1$, which generates a semicircular hump swept out by the initial data, here chosen to be

$$U = \begin{cases} 1, & -0.6 \le x \le -0.5, \\ 0 & \text{otherwise.} \end{cases} \tag{7.2}$$

Results are shown in Figures 2 and 3 on a fixed and moving mesh, respectively. Fastest convergence occurs when the sweeping is upwinded, taking into account the hyperbolic nature of the equation.

As expected, the solution on a fixed mesh is poor. On the other hand, when the mesh takes part in the minimization the norm $\mathcal{F}_1$ is driven down to machine accuracy. The redistribution effected by the least squares minimization forces global conservation and equidistributes ϕ amongst the triangles [1], leading to more uniform convergence. The cell edges have approximately aligned with characteristics in regions of nonzero ϕ, allowing a highly accurate solution to be obtained.

The left-hand graph in Figure 4 shows the convergence of the solution updating procedure using

(a) steepest descent globally with $\tau_1 = 0.5$;
(b) optimal local updates (quadratic model);
(c) optimal local updates over downwind cells only.

Convergence is improved in (b) and (c). Even though (c) is not monotonic it converges very quickly, albeit to a higher value, due to the minimization being constrained.

The convergence rates obtained when the nodes are allowed to move are shown in Figure 4 (right). Once again we start from the converged solution on the fixed grid and use

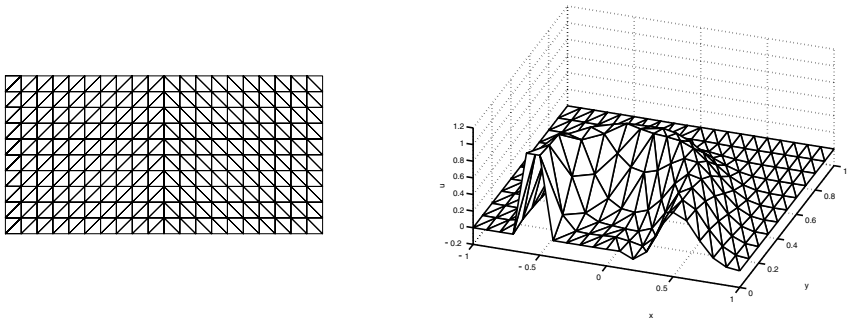

FIG. 2. *Initial grid and solution for Example* 1.

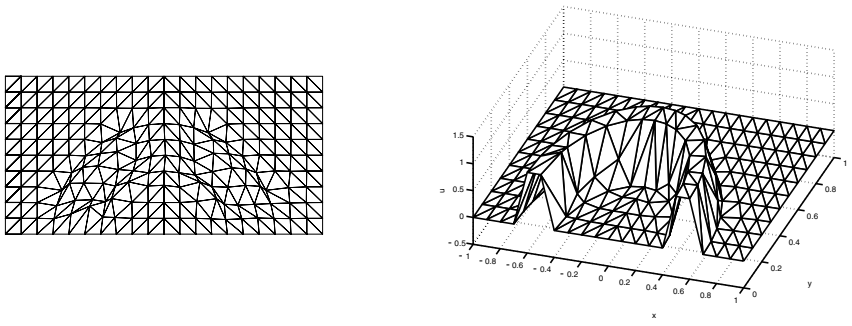

FIG. 3. *Final grid and solution for Example* 1.

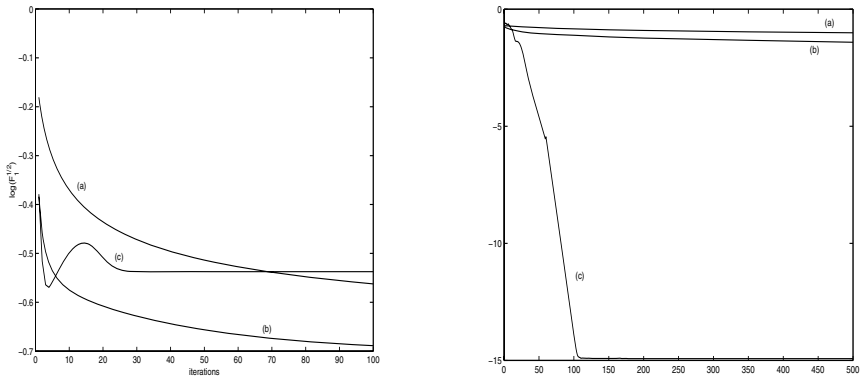

FIG. 4. *Comparisons of convergence histories.*

(a) steepest descent globally with $\tau_1 = 0.5$ and $\sigma_1 = 0.01$;
(b) Hessian local updates;
(c) Hessian local updates over downwind cells only.

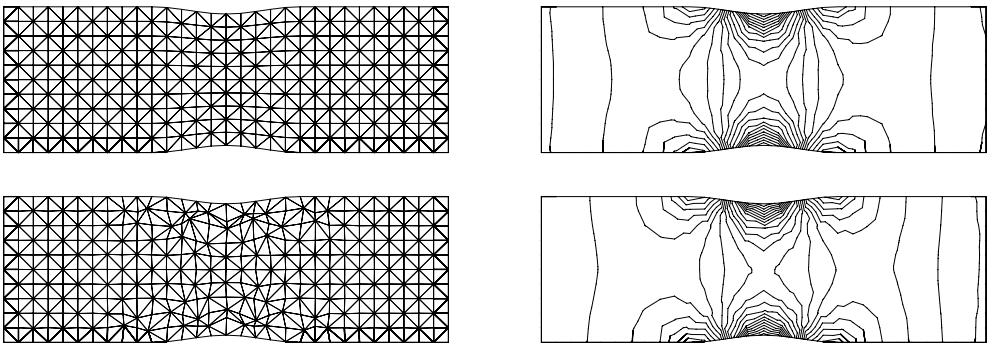

FIG. 5. *Initial grid and solution for Example* 2.

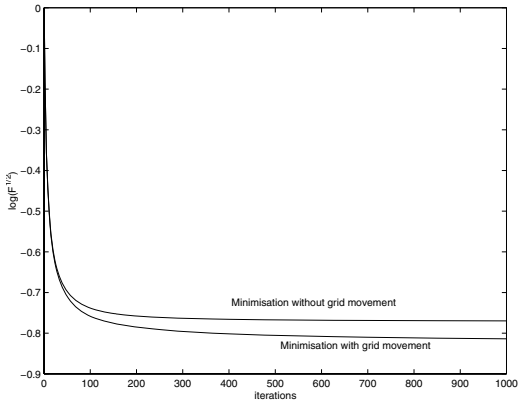

FIG. 6. *Convergence histories with and without mesh movement.*

A small amount of mesh smoothing was included in (b) and (c). In particular, (b) became stuck in a local minimum if more iterations were used. Node locking was a problem with the full least squares approach: node removal or steepest descent updates could be used to alleviate this problem but when tried these still took over 1000 iterations, so they were not competitive when compared to the upwinding approach, which yielded the best result.

Example 2. We now consider the system of equations (2.13) corresponding to a form of the homogeneous Shallow Water Equations written in conserved variables (see [5], [6]).

We shall consider a smooth subcritical constricted channel flow governed by these equations. The computational domain represents a channel of length 3 meters and width 1 meter with a 5% bump in the middle third. The freestream Froude number is defined to be $F_\infty = 0.25$, and the freestream depth is $h_\infty = 1m$. The resulting flow is entirely subcritical and symmetric about the center of the constriction (the narrowest point in the channel).

The fixed mesh is shown at the top of Figure 5 and the least squares descent solution (depth contours) on the mesh beneath it. This is also the initial mesh for the iteration when the mesh is moved. The other pictures in the figure show the adapted mesh and solution on this mesh.

Figure 6 shows convergence histories for this problem with and without mesh movement. An improved minimum is achieved by incorporating mesh movement in the minimization process. However, $\mathcal{F}_1$ is not dramatically decreased in this subcritical problem because there are no particularly sharp features in the flow which can be improved upon by the use of mesh movement.

8. Use of degenerate triangles. In the presence of shocks or contact discontinuities least squares methods give inaccurate solutions which are unacceptable. One way to combat this problem is to divide the region into a number of domains and introduce degenerate triangles at the interface, as suggested in [12]. We may then use a least squares method with moving nodes to adjust the position of the discontinuity, as in shock fitting methods.

Consider again consider the scalar problem (2.1) as a PDE generating a shock or contact discontinuity. We first obtain an initial approximate solution U to this equation by the use of a multidimensional upwinding shock capturing scheme. An initial discontinuous solution may then be constructed by introducing degenerate (vertical) triangles in the regions identified as shocks, using a shock identification technique. In the results shown below this step was carried out manually, but the degenerate triangles can be added automatically using techniques that exist in the shock fitting literature (see for example [16], [15]). The corners of the degenerate triangles are designated as shocked nodes, and these form an internal boundary, on either side of which the least squares method may be applied in two smooth regions where it is known to perform well. The position of the discontinuity can then be improved by minimizing a least squares shock monitor based either on the fluctuation in the degenerate cells or on the jump condition.

Then consider the jump condition at a shock associated with the conservation law (2.1),

$$\underline{f}(u_L).\underline{n}_L + \underline{f}(u_R).\underline{n}_R = 0, \tag{8.1}$$

where $\underline{f}(u_L)$ and $\underline{f}(u_R)$ are the fluxes to the left and right of a discontinuous edge.

We obtain an improved location of the discontinuity in the discretized problem by minimizing an L_2 measure of the residual of the jump condition with respect to node positions, using a piecewise linear approximation F to f. Thus consider minimization of the norm

$$\mathcal{F}_3 = \sum_{Q\in\Omega} \int_{\Gamma_Q} (\underline{F}(U_L).\underline{n}_L + \underline{F}(U_R).\underline{n}_R)^2 d\Gamma \tag{8.2}$$

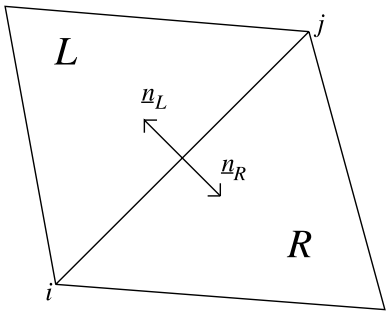

FIG. 7. *Cells on either side of a discontinuous edge.*

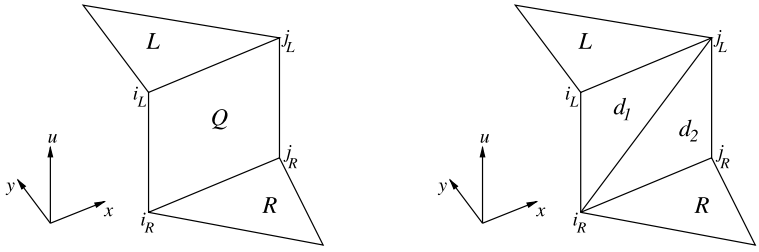

FIG. 8. *Degenerate quadrilaterals Q and triangles d_1, d_2.*

to update the position of the discontinuity where Γ_Q is the edge connecting nodes i and j in Figure 7, and $\underline{F}(U_L), \underline{F}(U_R)$ are the values of $\underline{F}$ at the left and right states.

We could have used an approximation based on degenerate triangles rather than quadrilaterals (see [4]). When updating the nodal positions $\underline{X}_{i_L}$ and $\underline{X}_{i_R}$ we require that they have the same update (so that the cell remains degenerate). The update comes from minimization with respect to their common position vector.

Consider the fluctuations ϕ_{d1} and ϕ_{d2} in the degenerate triangles d_1 and d_2 on the edge containing nodes i and j in Figure 8.

From (2.7) these are

$$\phi_{d_1} = -\frac{1}{2}\left[\underline{F}_i\right].\underline{n}_{i_L}, \qquad \phi_{d_2} = -\frac{1}{2}\left[\underline{F}_j\right].\underline{n}_{j_R}, \tag{8.3}$$

where the square bracket denotes the jump across the discontinuity. The contributions from two edges vanish in each case due to the degeneracy of the triangles.

Then

$$\phi_{d_1}^2 + \phi_{d_2}^2 = \frac{1}{4}\left\{\left([\underline{F}_i].\underline{n}_{i_L}\right)^2 + \left([\underline{F}_j].\underline{n}_{j_L}\right)^2\right\}, \tag{8.4}$$

and so we can also use

$$\mathcal{F}_4 = \sum_{e\in\Omega_D} \phi_e^2 \tag{8.5}$$

to improve the position of the shock, where Ω_D is the set of degenerate triangles. (Note that $\mathcal{F}_4$ is bounded because ϕ_e in (2.3) is always bounded, even at shocks where U is discontinuous. On the other hand, the average residual, given by (2.4), is not bounded since $S_e = 0$ at shocks.)

A descent least squares method can then be used on $\mathcal{F}_3$ or $\mathcal{F}_4$ to move the shocked nodes into a more accurate position, keeping the u_L and u_R values fixed. The procedure may be interleaved with a descent least squares method on $\mathcal{F}_1$ or $\mathcal{F}_2$ for the smooth solution on either side.

We now give some numerical results using this technique.

9. Numerical results for discontinuous solutions. We now show results from three problems which exhibit discontinuities, one scalar and the others for different nonlinear systems.

Example 3. The first of these problems is the advection of a contact discontinuity. We consider circular advection as in Example 1 but with initial data

$$U = \begin{cases} 1, & x \le -0.5, \\ -1, & x \ge -0.5 \end{cases} \tag{9.1}$$

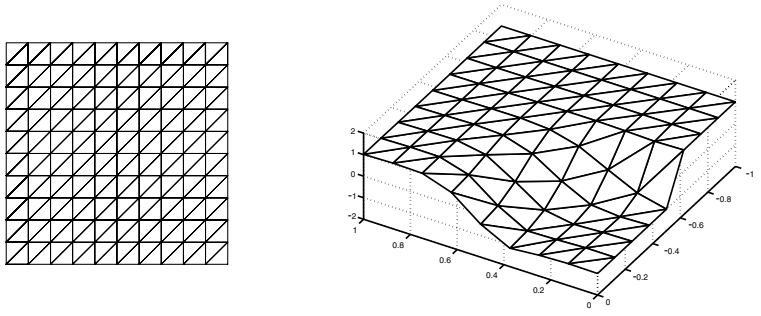

FIG. 9. *Fixed mesh and solution for Example* 3.

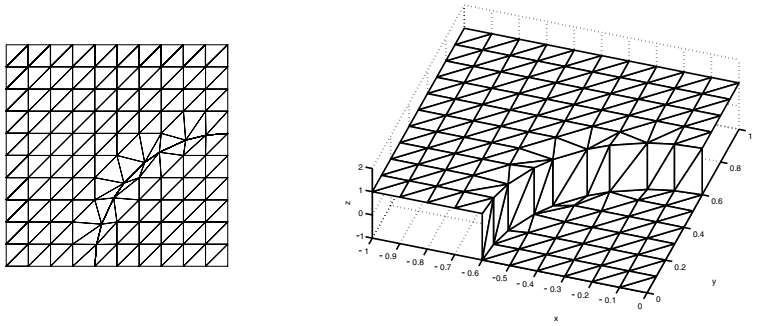

FIG. 10. *Moved mesh and solution for Example* 3.

on the inflow side. This represents the circular advection of a contact discontinuity.

Degenerate triangles are inserted vertically to connect the triangles on either side of the discontinuity. The solution updates come from a least squares descent method taken over nondegenerate elements. (The least squares updates to the solution come from nondegenerate elements.) The shock node adaptation is by the mimimization of F_4 (see (8.5)). Results are shown in Figures 9 and 10 for a fixed mesh and a moving mesh using degenerate triangles. Convergence histories are shown in Figure 11. The contact discontinuity has been accurately located through the use of the degenerate elements.

Example 4. Consider again the Shallow Water Equations system of Example 2. The problem which interests us here is that of a transcritical constricted channel flow which exhibits a hydraulic jump in the constriction. The computational domain represents a channel of length 3 meters and width 1 meter with a 10% bump in the middle third. The freestream Froude number is defined to be $F_\infty = 0.55$, the freestream depth is $h_\infty = 1m$, and the freestream velocity is given by $(u_\infty, v_\infty) = (1.72, 0)$.

An initial solution for the least squares shock fitting approach is found by the elliptic-hyperbolic Lax–Wendroff multidimensional upwinding scheme of Mesaros and Roe; see [8]. This time we seek to locate the hydraulic jump by adding degenerate quadrilaterals at the approximate position of the shock and seeking the best position of the shocked nodes. This is again achieved by using a least squares descent method on $\mathcal{F}_4$ with degenerate triangles to improve the position of the shock. Virtually identical results are obtained using $\mathcal{F}_3$ with quadrilaterals.

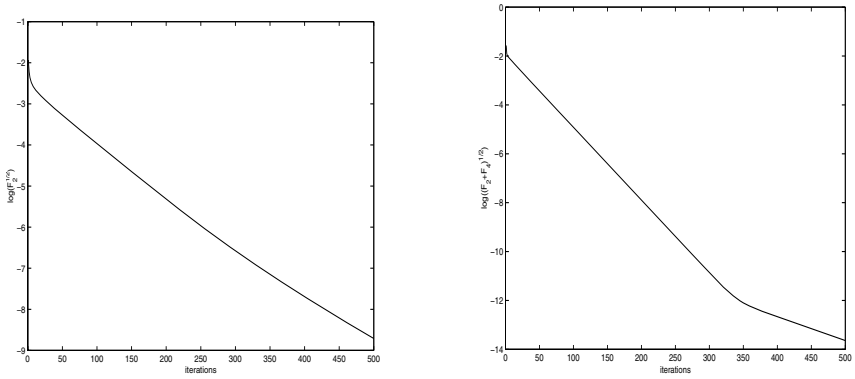

FIG. 11. *Convergence histories.*

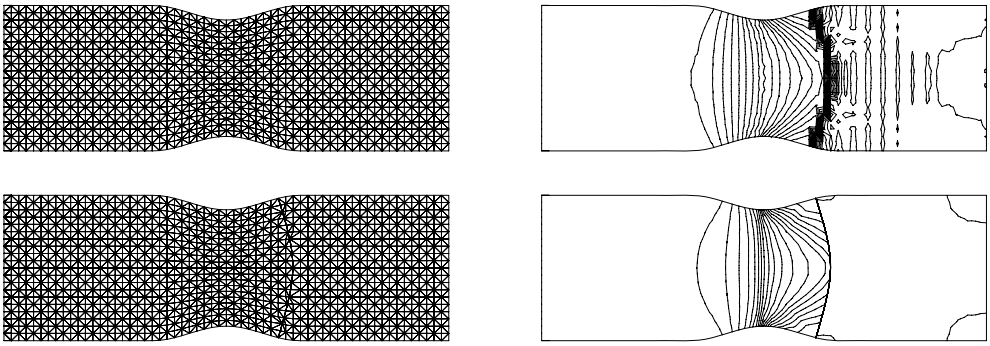

FIG. 12. *Results for Example* 4.

Results are shown in Figure 12, which shows the meshes and solution depth contours obtained. A bow-shaped hydraulic jump which is strongest at the boundaries is predicted, which agrees with solutions obtained using a shock capturing solution on a very fine mesh. Here it is achieved at little cost. Note not only the better shock resolution but also the much cleaner post-shock solution.

Example 5. Finally we consider the system (2.13) again but this time corresponding to the Euler equations of gasdynamics written in conserved variables [5].

This example is chosen to exhibit the shock fitting capabilities of the method for a purely supersonic flow which has an exact solution [17]. The computational domain is of length 3 meters and width 1 meter. Supersonic inflow boundary conditions, given by

$$\begin{aligned} \underline{U}(0,y) &= (1.0, 2.9, 0, 5.99073)^t, \\ \underline{U}(x,1) &= (1.69997, 4.45280, -0.86073, 9.87007)^t, \end{aligned} \tag{9.2}$$

are imposed on the left and upper boundaries, respectively. At the right-hand boundary supersonic outflow conditions are applied, while the lower boundary is treated as a solid wall.

The boundary conditions are chosen so that the shock enters the top left-hand corner at an angle of 29^o to the horizontal and is reflected by a flat plate on the lower boundary. The flow in regions away from shocks is constant. The same strategy is

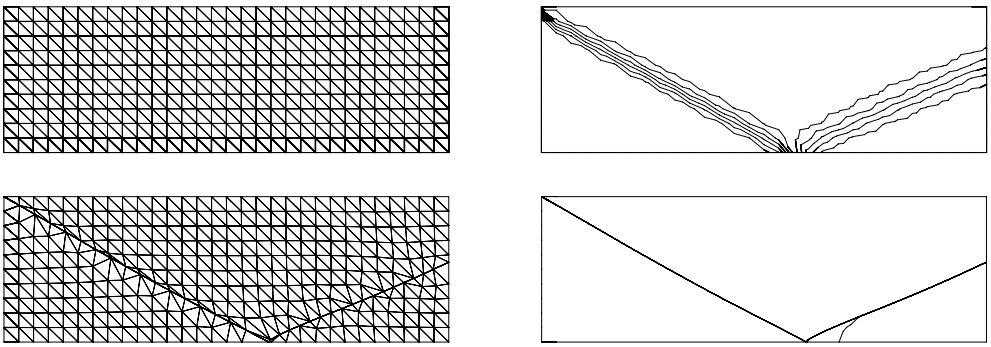

FIG. 13. *Results for Example* 5.

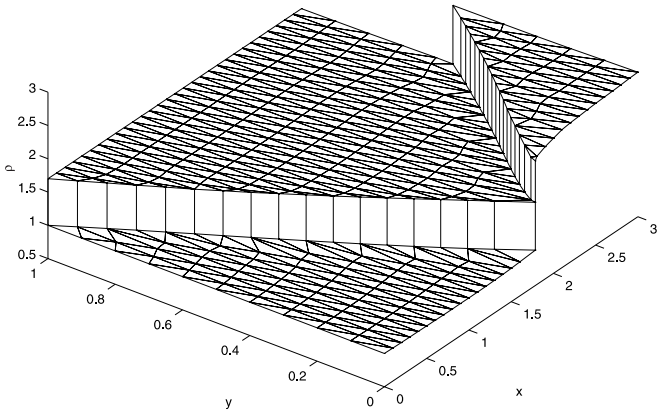

FIG. 14. *Solution (density) in* 3*D.*

employed as in the previous example, including the same shock capturing scheme, with the results shown in Figure 13, where the density contours are plotted. The predicted shock comes in from the top left hand at an angle of 29.2^o to the horizontal, and the solution is virtually constant apart from the discontinuities, in close agreement with the analytic solution (see Figure 14).

The angle made by the reflected shock with the horizontal is also in line with the theory. (See [14], which gives the angle as 23.3°.)

10. Conclusion. In this paper we have considered the approximate solution of steady first order PDEs by a least squares finite volume fluctuation distribution scheme with mesh movement. On fixed meshes, by the nature of the fluctuation distribution technique, the fluctuations on triangular meshes are not driven to zero. The solution may be improved by introducing extra degrees of freedom by adding node locations to the list of unknowns and moving the mesh. As a result, for scalar problems the fluctuations are driven down to zero (to machine accuracy), while for systems of equations the errors are much reduced. The descent least squares procedure with mesh movement also induces global conservation and equidistributes the fluctuation amongst the triangles, thus proceeding down to the steady limit in a uniform way.

For scalar problems convergence can be greatly accelerated by carrying out the

iterations in an upwind manner.

For problems with discontinuities the descent least squares method does not give good solutions, but the mesh movement technique enables improvement of the location of the discontinuity in a manner akin to shock fitting. By minimizing a measure of the jump condition an approximate position of the shock can be maneuvered into an accurate position. This allows the descent least squares method to be used on either side of the shock to gain a good approximation of the smooth regions of the flow.

Acknowledgment. The authors wish to thank Phil Roe of the University of Michigan for many helpful suggestions while visiting the University of Reading under an EPSRC Visiting Fellowship.

REFERENCES

[1] M. J. Baines, *Least-squares and approximate equidistribution in multidimensions*, Numer. Methods Partial Differential Equations, 15 (1999), pp. 605–615.

[2] M. J. Baines and M. E. Hubbard, *Multidimensional upwinding with grid adaptation*, in Numerical Methods for Wave Propagation, E. F. Toro and J. F. Clarke, eds., Kluwer Academic Publishers, Dordrecht, The Netherlands, 1998, pp. 33–54.

[3] M. J. Baines and S. J. Leary, *Fluctuation and signals for scalar hyperbolic equations on adjustable meshes*, Comm. Numer. Methods Engrg., 15 (1999), pp. 877–886.

[4] M. J. Baines, S. J. Leary, and M. E. Hubbard, *A finite volume method for steady hyperbolic equations*, in Finite Volumes for Complex Applications II, R. Vilsmeier, F. Benkhaldoun, and D. Hanel, eds., Hermes, Paris, 1999, pp. 787–794.

[5] M. E. Hubbard, *Multidimensional Upwinding and Grid Adaptation for Conservation Laws*, Ph.D. Thesis, University of Reading, UK, 1996.

[6] M. E. Hubbard and M. J. Baines, *Conservative multidimensional upwinding for the steady two-dimensional shallow water equations*, J. Comput. Phys., 138 (1997), pp. 419–448.

[7] S. J. Leary, *Least Squares Methods with Adjustable Nodes for Steady Hyperbolic PDEs*, Ph.D. Thesis, University of Reading, UK, 1999.

[8] L. M. Mesaros and P. L. Roe, *Multidimensional fluctuation splitting schemes based on decomposition methods*, in Proceedings of the 12th AIAA CFD Conference, San Diego, 1995.

[9] K. Miller and M. J. Baines, *Least squares moving finite elements*, IMA J. Numer. Anal., 21 (2001), pp. 621–642.

[10] P. L. Roe, *Fluctuation and signals: A framework for numerical evolution problems*, in Proceedings of IMA Conference on Numerical Methods for Fluid Dynamics, Reading, UK, 1982, Academic Press, London, 1982, pp. 219–257.

[11] P. L. Roe, *Compounded of many simples*, in Barriers and Challenges in Computational Fluid Dynamics, V. Ventakrishnan, M. D. Salas, and S. R. Chakravarthy, eds., Kluwer Academic Publishers, Dordrecht, The Netherlands, 1998, pp. 241–258.

[12] P. L. Roe, *Fluctuation Splitting on Optimal Grids*. AIAA paper 97-2034, 1997.

[13] R. Struijs, P. L. Roe, and H. Deconinck, *Fluctuation splitting schemes for the 2-D Euler equations*, in Computational Fluid Dynamics 1991-01, VKI Lecture Series, 1991.

[14] F. Taghaddosi, W. G. Habashi, G. Guevremont, and D. Alt-Ali-Yahia, *An Adaptive Least Squares Method for the Compressible Euler Equations*, AIAA paper 97-2097, 1997.

[15] J. Y. Trepanier, M. Paraschivoiu, M. Reggio, and R. Camarero, *A conservative shock fitting method on unstructured grids*, J. Comput. Phys., 126 (1996), pp. 421–433.

[16] J. Van Rosendale, *Floating shock fitting via Lagrangian adaptive meshes*, in Proceedings of the 12th AIAA CFD Conference, San Diego, 1995.

[17] H. Yee, R. F. Warming, and A. Harten, *Implicit total variation diminishing (TVD) schemes for steady state calculations*, J. Comput. Phys., 57 (1985), pp. 327–366.